

# Large Eddy Simulation of Three-Stream Jets

J. Xiong<sup>1</sup>, F. Liu<sup>2</sup>, and D. Papamoschou<sup>3</sup>  
*University of California, Irvine, Irvine, CA, 92697*

We present a computational study of three-stream jets simulating the exit conditions of future commercial supersonic aircraft engines. The study is conducted for coaxial and asymmetric configurations at realistic cycle condition. The asymmetric arrangement involved offsetting the tertiary duct and applying an internal wedge-shape deflector. Computations using Large Eddy Simulation (LES) provide detailed time-resolved information on the flow field. The resulting statistics are compared with the output of a Reynolds-Averaged Navier-Stokes (RANS) solver, a low-cost method that can be used as a design tool. The statistics are in overall agreement, with RANS predicting a slightly longer potential core than LES. The asymmetry produces significantly thickened tertiary flow and turbulent kinetic energy reduction on the underside of the jet plume with attendant specific thrust loss of only 0.039%. The far field noise is calculated by applying the Ffcows Williams-Hawkings (FWH) equation to the LES results. The results show similar trends of far field noise spectra as measured by experiments.

## I. Introduction

Over the past twenty years, Large Eddy Simulation (LES) and Detached Eddy Simulation (DES) of turbulent flows, coupled with integral acoustics methods, such as Kirchhoff and Ffcows Williams-Hawkings, have made significant progress towards noise prediction and exploration of the relevant flow physics. Applications have included single- and dual-streams jets<sup>1-7</sup>. On the other hand, these techniques are computationally very expensive and cannot be considered as design tools. Applied to selected configurations, they can provide time-resolved information that would be very difficult to measure

---

<sup>1</sup> Associate Specialist, Department Mechanical and Aerospace Engineering, jxiong@uci.edu, AIAA Member

<sup>2</sup> Professor, Department Mechanical and Aerospace Engineering, fliu@uci.edu, AIAA Fellow.

<sup>3</sup> Professor, Department Mechanical and Aerospace Engineering, dpapamos@uci.edu, AIAA Fellow.

experimentally. This information is then used to inform and validate low-cost Reynolds Averaged Navier Stokes (RANS) predictions, which can then be connected to acoustics via acoustic analogies.

Our UCI aeroacoustics research group has presented a broad parametric experiment study of three-stream jets compatible with engines of supersonic transports with coaxial and asymmetric configurations<sup>8</sup>. We have shown that the asymmetric delivery of the tertiary stream shows strong potential for noise reduction. In order to fully understand the noise reduction mechanism and enable to build a fast and accurate quantitative noise prediction model, a computation study of three-stream jet using LES and RANS has been conducted. The present paper reports the computational results of coaxial and asymmetric nozzles with LES and RANS. First, the RANS computational code was validated against experimental data on the mean velocity of the jet at cold condition. Thereafter the comparisons of the simulation results of time-average velocity and turbulent kinetic energy fields of the jets at cycle point hot between LES and RANS are performed. Finally, the far field noise prediction was calculated using FWH equation<sup>9</sup>.

## **II. Computational Approach**

### **A. Numerical Code**

The computational fluid dynamics code used here is known as PARCAE<sup>10</sup> and solves the unsteady three-dimensional Navier-Stokes equations on structured multiblock grids using a cell-centered finite-volume method. Information exchange for flow computation on multiblock grids using multiple CPUs is implemented through the MPI (Message Passing Interface) protocol. In its unsteady implementation, the solver uses implicit backward three-layer second-order time integration with explicit five stage Runge-Kutta dual time stepping with local time stepping, residual smoothing, and multigrid techniques for convergence acceleration.

In the RANS simulation the Jameson-Schmidt-Turkel dissipation scheme<sup>11</sup> and Shear Stress Transport (SST) turbulence model of Menter<sup>12</sup> were used. The SST model combines the advantages of the  $k-\omega$  and  $k-\epsilon$  turbulence models for both wall-bounded and free-stream flows. Only the steady-state solution was

considered because we are interested in the time-averaged features of the flow. The RANS solver has been used in past research on dual-stream jets, and its predictions have been validated against mean velocity measurements performed at UCI<sup>13</sup> for dual stream jets.

In the LES, the time-evolving jet flow is simulated using a hybrid RANS/LES approach<sup>14, 15</sup>. The spatial discretization of the inviscid flux is based on the weighted averaged flux-difference splitting algorithm of Roe scheme<sup>16</sup>. The viscous flux is discretized using a second-order central difference scheme. Near the wall region the Spalart-Allmaras turbulence model<sup>17</sup> is used to model the turbulent viscosity, while in the free shear flow the computation relies on the subtle dissipation of the upwind scheme, using the method proposed by Shur et al<sup>14</sup>. The current LES solver has been successfully used in the Ma=0.9 single stream jet simulation<sup>18</sup>.

## B. Computational Model and Grid

The computation were performed for coaxial and asymmetric three-stream nozzles used in UCI subscale experimental investigation. The asymmetric arrangement involved offsetting the tertiary duct and applying an internal wedge-shaped deflector. The nozzles constructions are shown in Fig. 1. The tertiary nozzle exit diameter is  $D_t=38.1\text{mm}$ .

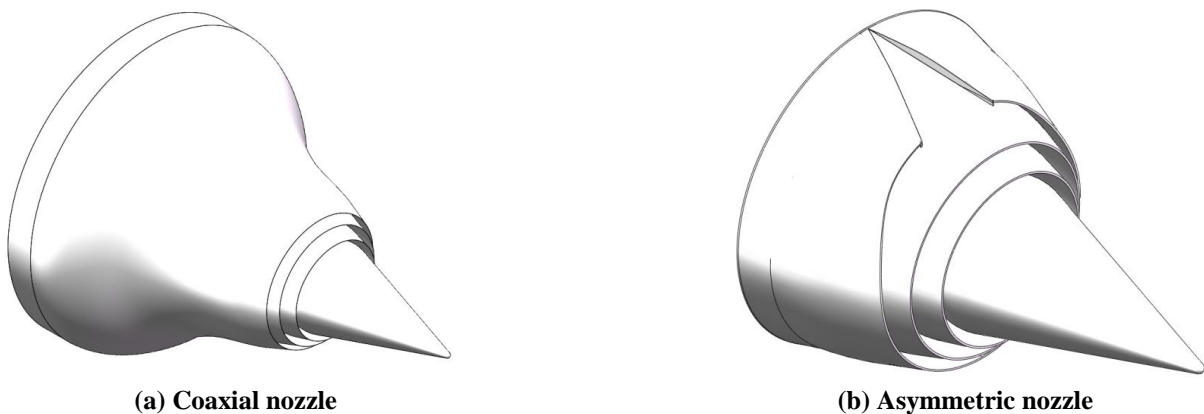
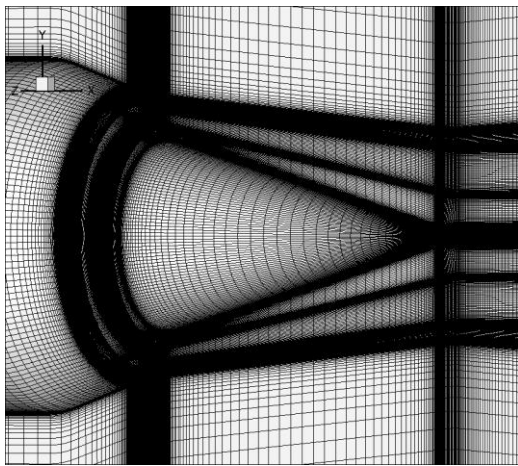


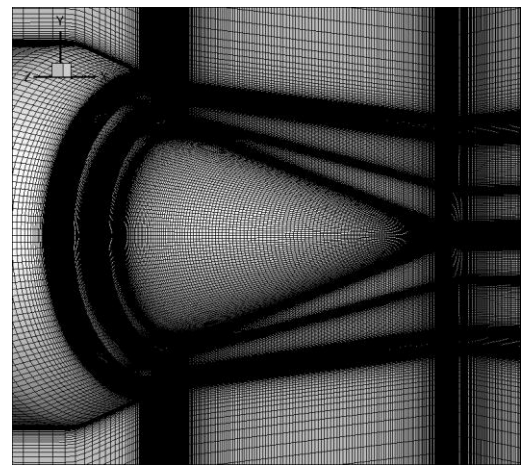
**Fig. 1 Three-stream nozzles.**

The computations encompassed both the internal nozzle flow as well as the external plume. Figure 2 shows the grids for coaxial nozzle in the vicinity of the nozzle exit for RANS and LES simulation

separately. The RANS mesh had about 8 million grid points. The computational domain extended to 30 jet diameters downstream and 5 diameters radially outward from the nozzle centerline. As the coaxial and asymmetric nozzles are symmetric around the  $x$ - $y$  plane, only one-half of the nozzle was modeled to save computational expense for the RANS simulation. For the LES mesh, the computational domain extended to 60 jet diameters downstream and 15 diameters radially. In order to fully resolve the fluctuation along the azimuthal direction whole nozzle was modeled. More grid points along streamwise direction are used to resolve the small scale eddies evolution. The grid contained about 44 million grid points. The grids were divided into multiblocks to implement parallelization on multiprocessors computers to reduce the convergence time.



(a) RANS mesh



(b) LES mesh

**Fig. 2 Computational grid.**

### **C. Flow and Boundary Conditions**

The flow conditions in the computations simulated those in subscale experiments conducted in our facilities. The nozzle exhaust condition are listed in the Table 1 and Table 2. The Reynolds number of the jet, based on tertiary diameter, were  $0.68 \times 10^6$  for the hot jets and  $0.35 \times 10^6$  for the cold jets.

**Table 1. Exhaust Cold Condition**

Stream	NPR	NTR	Velocity (m/s)
Primary	1.893	1	311.6
Secondary	1.268	1	195.5
Tertiary	1.145	1	148.7

**Table 2. Exhaust Hot Condition (cycle point)**

Stream	NPR	NTR	Velocity (m/s)
Primary	2.065	3.198	590.5
Secondary	2.028	1.285	370.1
Tertiary	1.534	1.185	281.9

For the primary, secondary, and tertiary duct flows, uniform total pressure and total temperature was specified at the inlet surface corresponding to the perfectly expanded exit Mach number. For the ambient region surrounding the nozzle flow, a characteristic boundary condition was defined, and the downstream static pressure was set to the ambient pressure. Adiabatic no-slip boundary condition was specified on all nozzle walls.

### III. Results

First, the RANS computational code was validated against experimental data on the mean velocity of the jet at cold condition. Thereafter the comparisons of the simulation results of time-average velocity and turbulent kinetic energy fields of the jets at cycle point hot between LES and RANS are performed. Finally, the far field noise prediction was calculated using FWH equation.

#### A. Cold jet results

To assess the accuracy of the RANS predictions, computations and experiments were performed for jet flows at cold conditions, using pure air in all streams. The use of cold conditions is necessitated by the availability of mean velocity diagnostics, which are restricted to the Pitot rake described in Ref. 13. Comparisons of computational and experimental distributions of the mean axial velocity  $u$ , plotted in Figures 3 through 6 for coaxial nozzle and Figures 7 through 10 for asymmetric nozzle. Figure 3 and

Figure 7 show the mean axial velocity on the symmetry plane for the coaxial and asymmetric nozzles at cold condition. Figure 4 and Figure 8 show the mean axial velocity on cross-sectional planes for the two nozzles. Figure 5 and Figure 9 show the mean axial velocity on the center line and maximum velocity for the two nozzles. Figure 6 and Figure 10 show the transverse distribution of the mean axial velocity on the symmetry plane at three axial stations for the two nozzles. The mean axial velocity comparisons show that the RANS results match the experimental trends with reasonable accuracy.

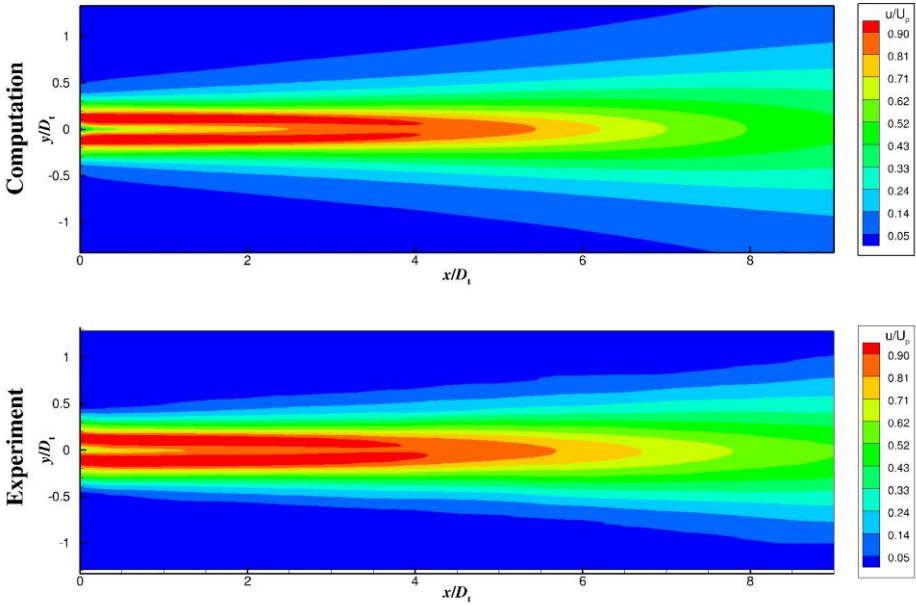


**Fig. 3** Distribution of mean axial velocity on the symmetry plane of cold jet issuing from coaxial nozzle.

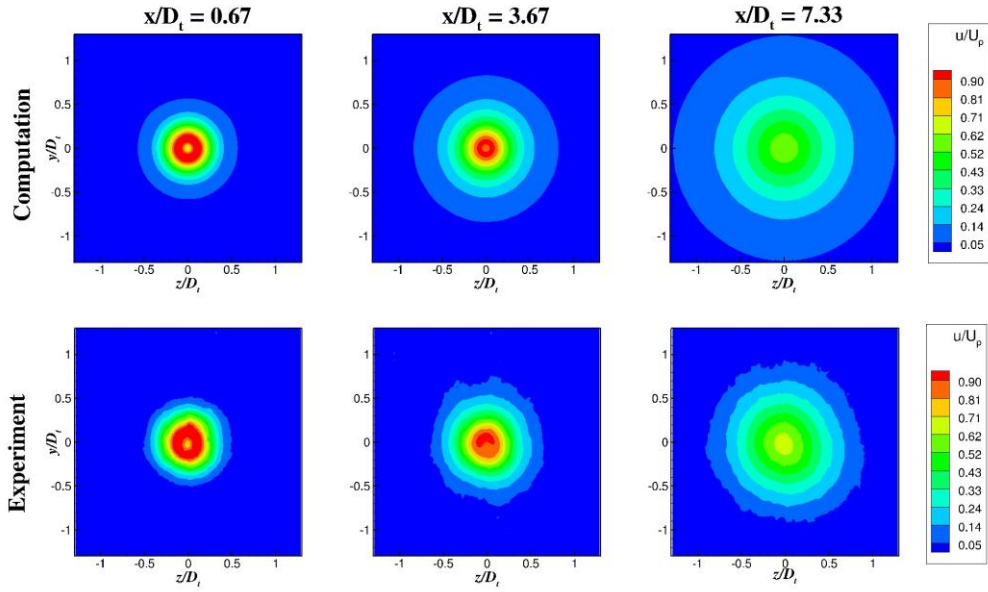


Fig. 4 Distribution of mean axial velocity on cross-sectional planes of cold jet issuing from coaxial nozzle

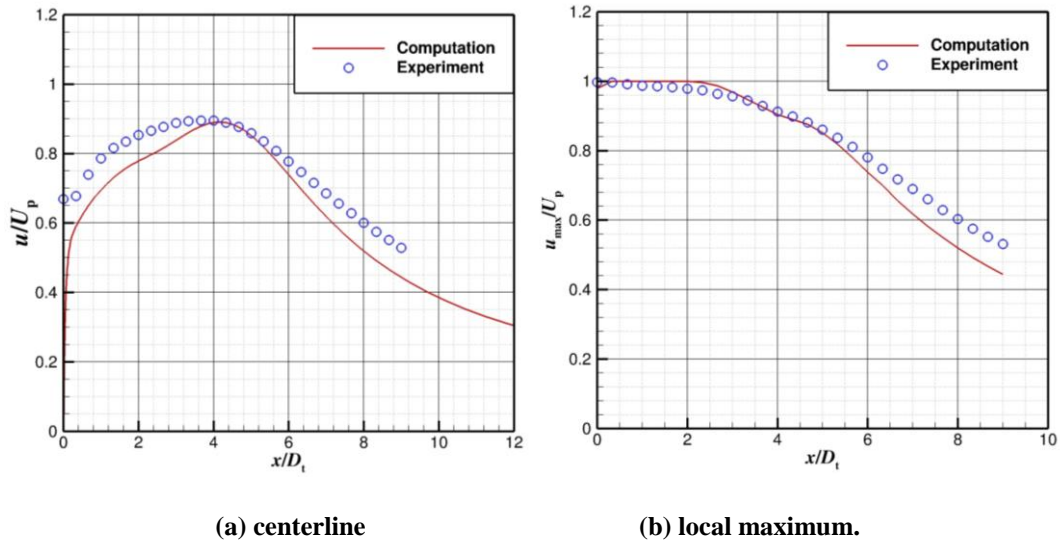
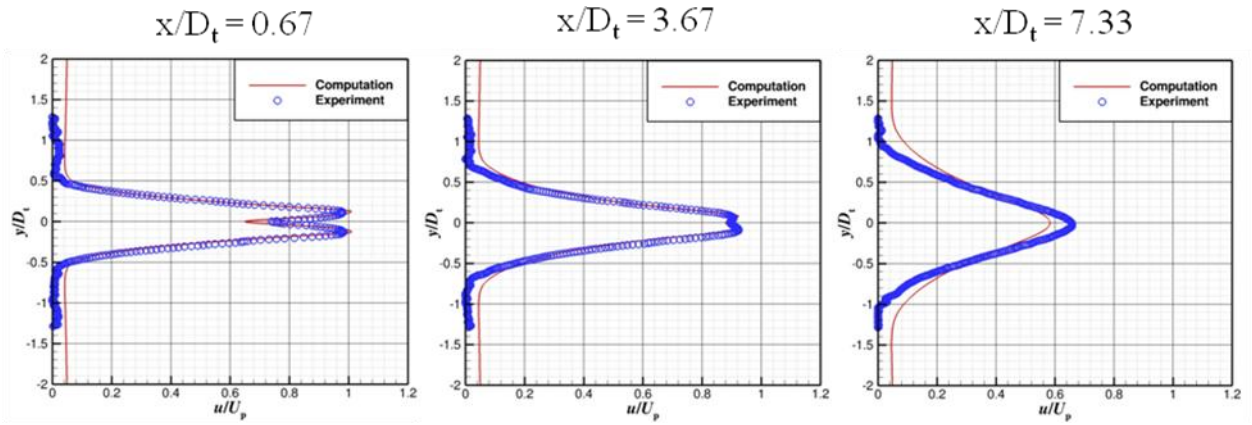
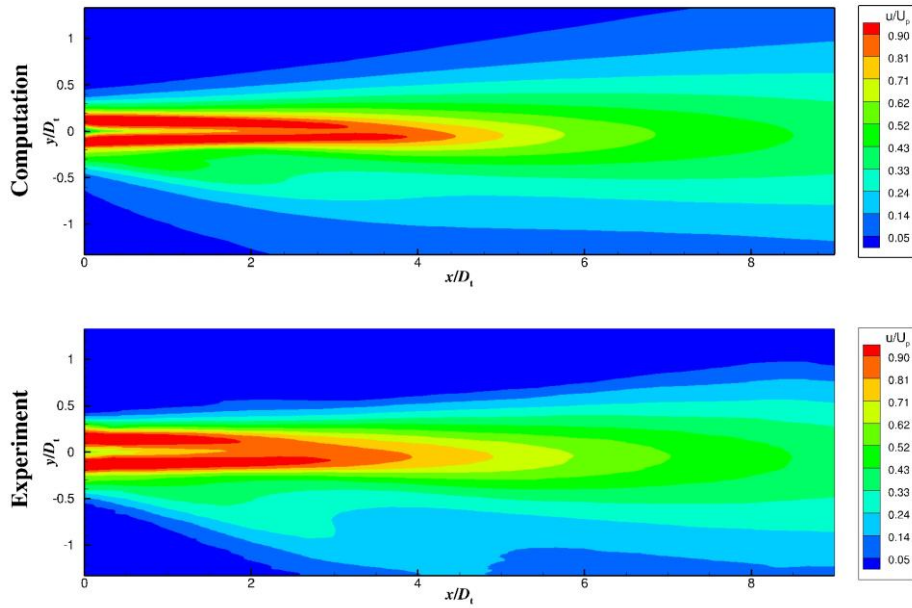


Fig. 5 Experimental (blue circles) and RANS (red line) axial distributions of normalized mean axial velocity  $u/U_p$  for coaxial nozzle.



**Fig. 6** Experimental (blue circles) and RANS (red line) transverse distributions of normalize mean axial velocity  $u/U_p$  on the symmetry plane and axial stations  $x/D_t = 0.67, 3.67,$  and  $7.33$  for coaxial nozzle.



**Fig. 7** Distribution of mean axial velocity on the symmetry plane of cold jet issuing from asymmetric nozzle.

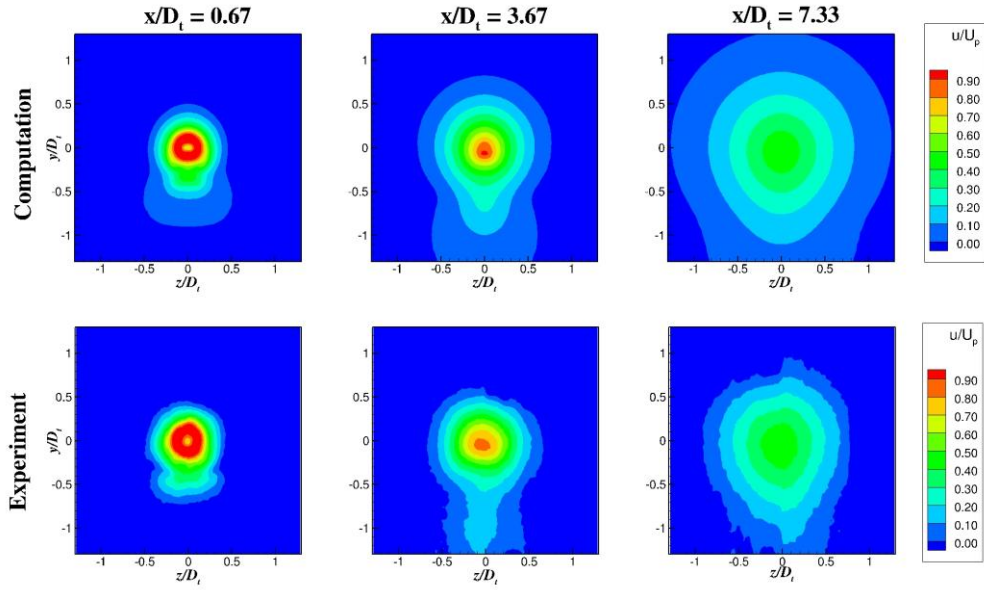


Fig. 8 Distribution of mean axial velocity on cross-sectional planes of cold jet issuing from asymmetric nozzle.

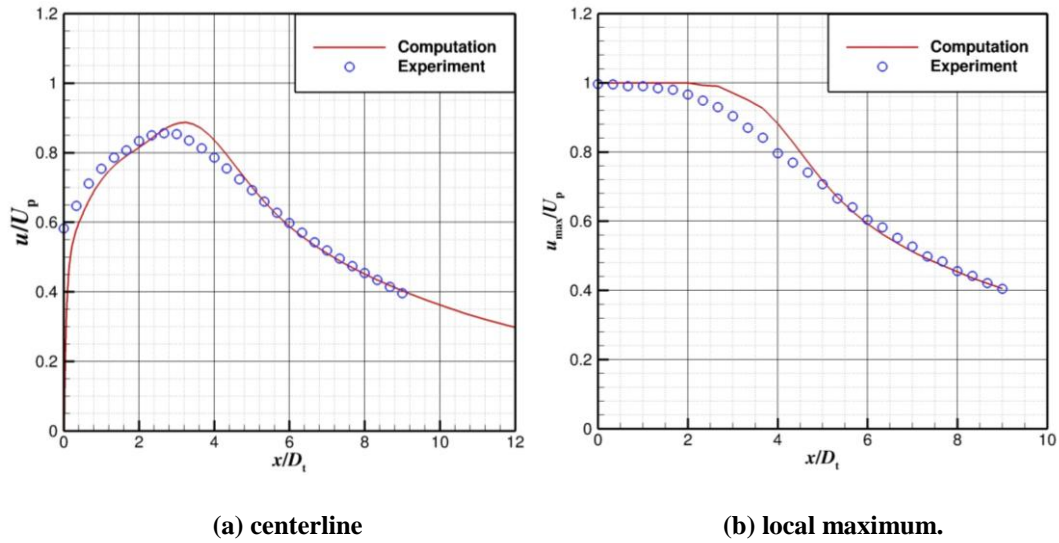
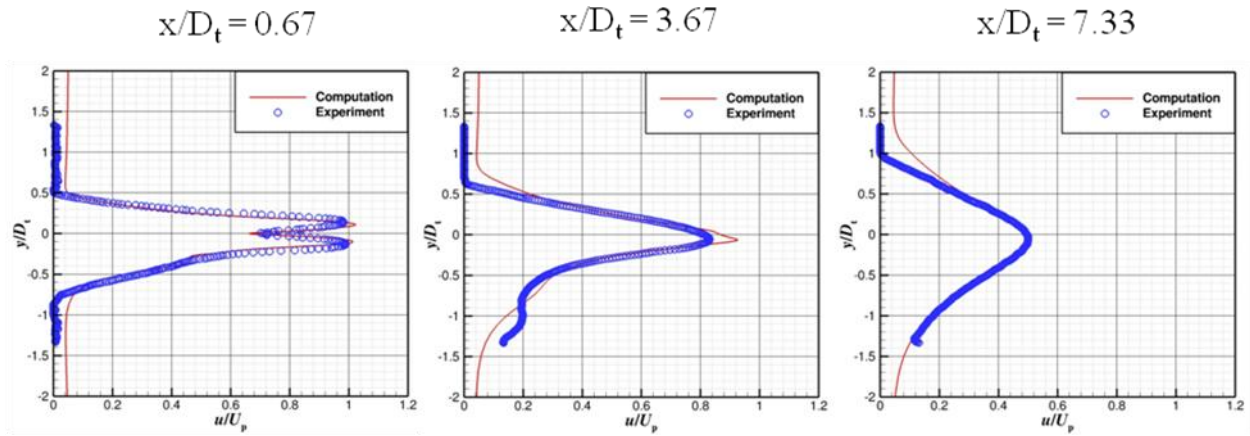


Fig. 9 Experimental (blue circles) and RANS (red line) axial distributions of normalized mean axial velocity  $u/U_p$  for asymmetric nozzle



**Fig. 10** Experimental (blue circles) and RANS (red line) transverse distributions of normalized mean axial velocity  $u/U_p$  on the symmetry plane and axial stations  $x/D_t = 0.67, 3.67,$  and  $7.33$  for asymmetric nozzle

## B. Hot jet time-averaged results

In this session, the presentation of the results shows the comparison of time-averaged velocity fields between LES and RANS for the coaxial and asymmetric configurations at hot condition. Figure 11 shows the time-averaged fields of the time-averaged axial velocity on the symmetry plane using the LES and RANS approaches. Figure 12 shows the time-averaged axial velocity contours on three transverse planes. Figure 13 shows the centerline time-averaged axial velocity distribution. Although the RANS computation predicts a slightly longer potential cores than the LES computation, the two approaches show similar flow field patterns and trends. Both methods predict the same velocity decay rate after the velocity peak and capture the thickening of the tertiary stream on the underside of the core and second streams and the distortion of the transverse plane contours from circular to oval.

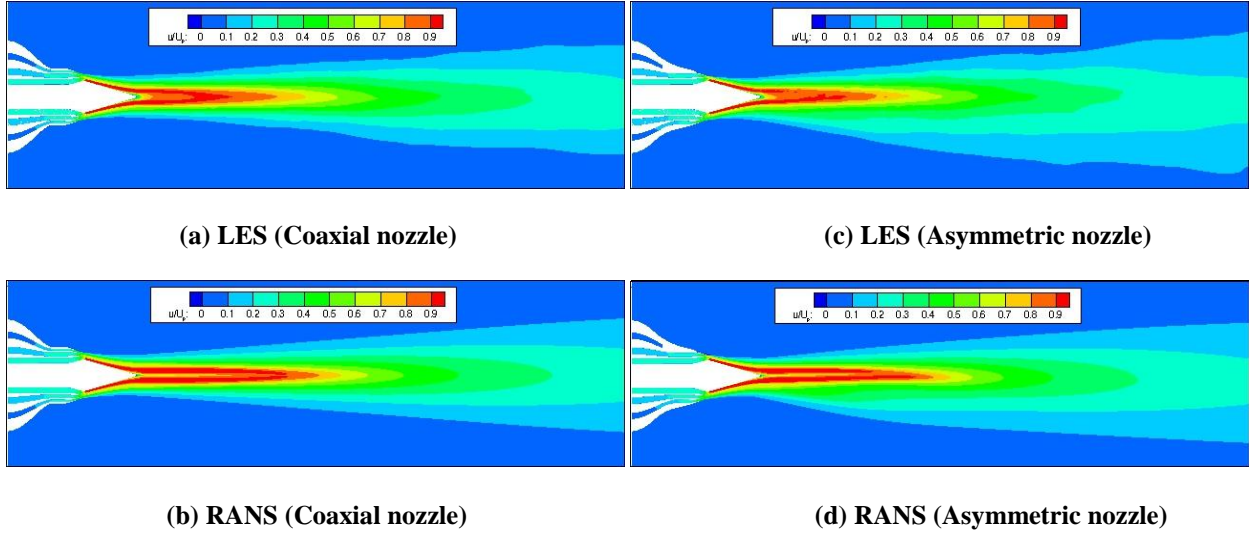
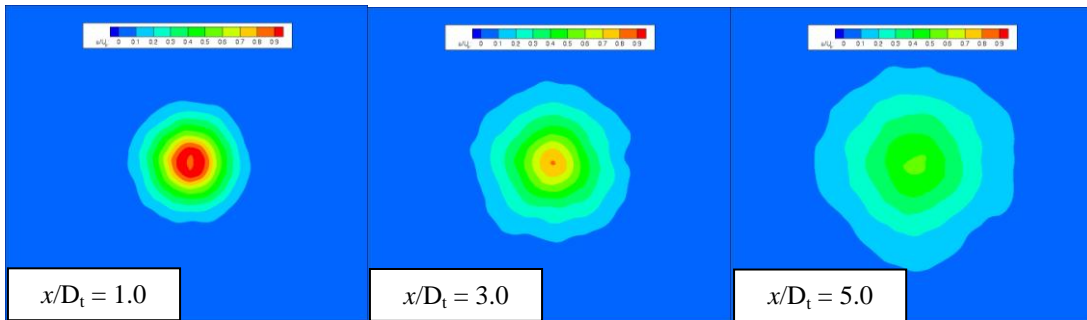
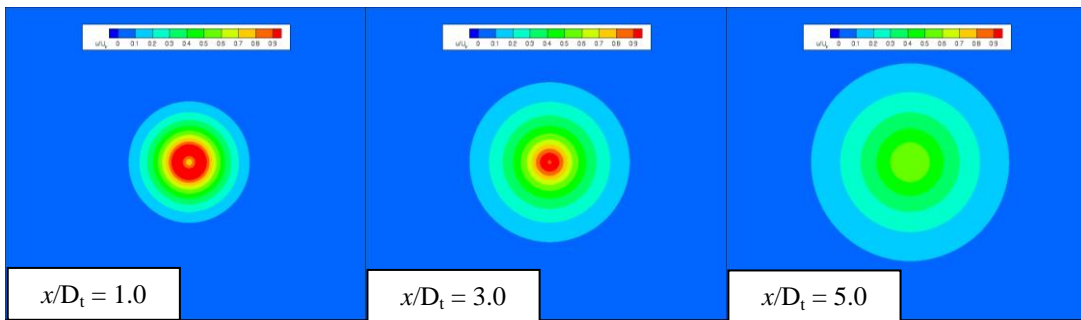


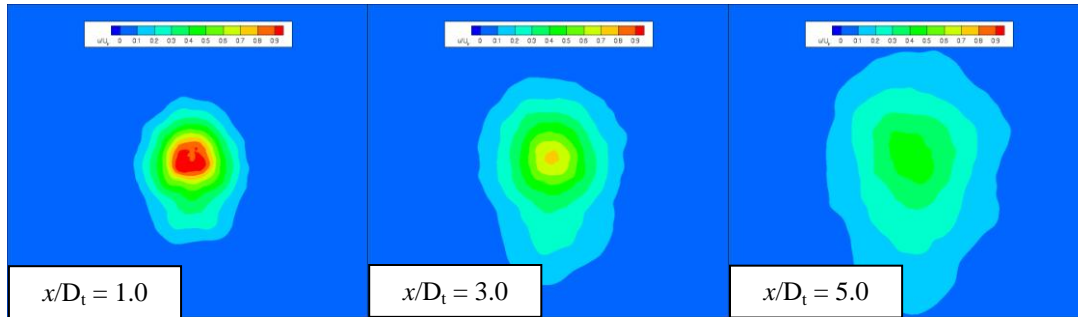
Fig. 11 Contours of mean axial velocity on the symmetry plane for the three stream jets. Left column shows the coaxial nozzle. Right column shows the asymmetric nozzle.



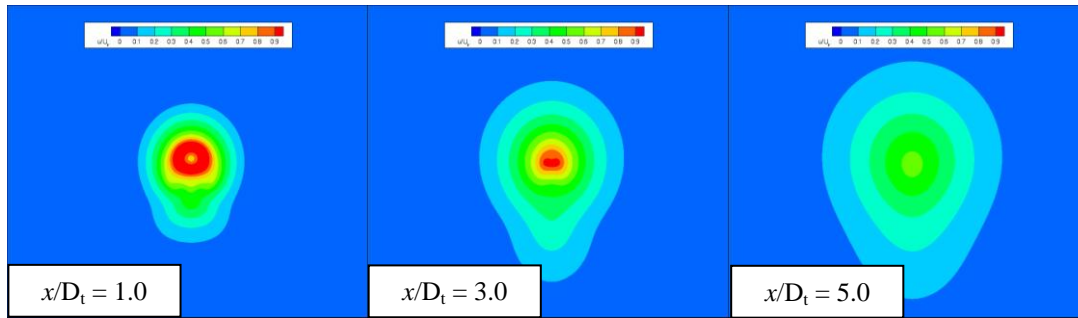
(a) LES (Coaxial nozzle)



(b) RANS (Coaxial nozzle)

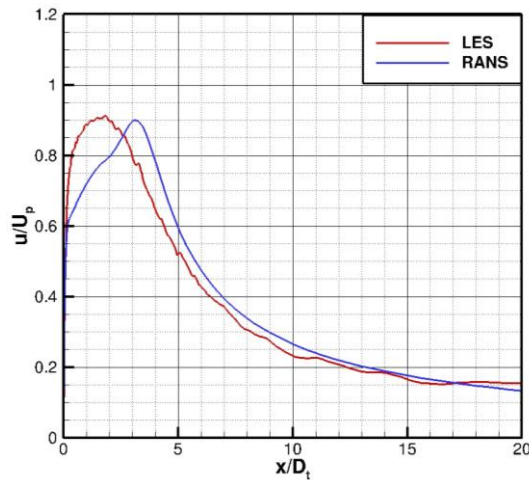


(c) LES (Asymmetric nozzle)

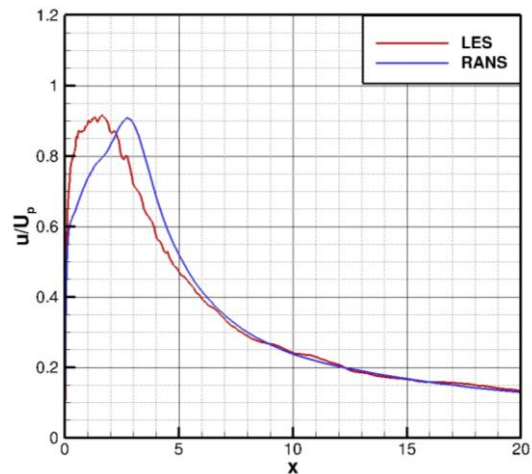


(d) RANS (Asymmetric nozzle)

Fig. 12 Contours of mean axial velocity on transverse planes.



(a) Coaxial nozzle

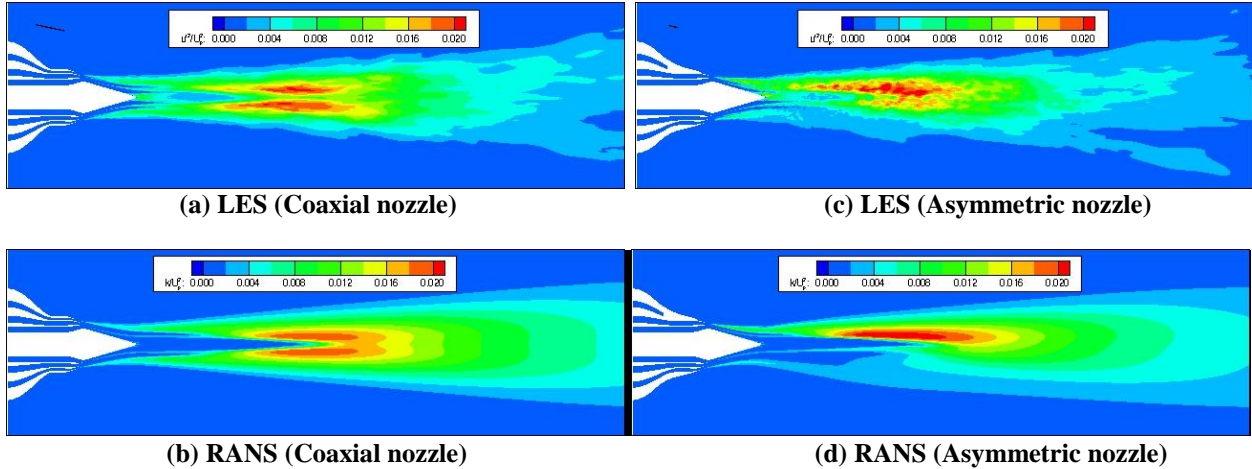


(b) Asymmetric nozzle

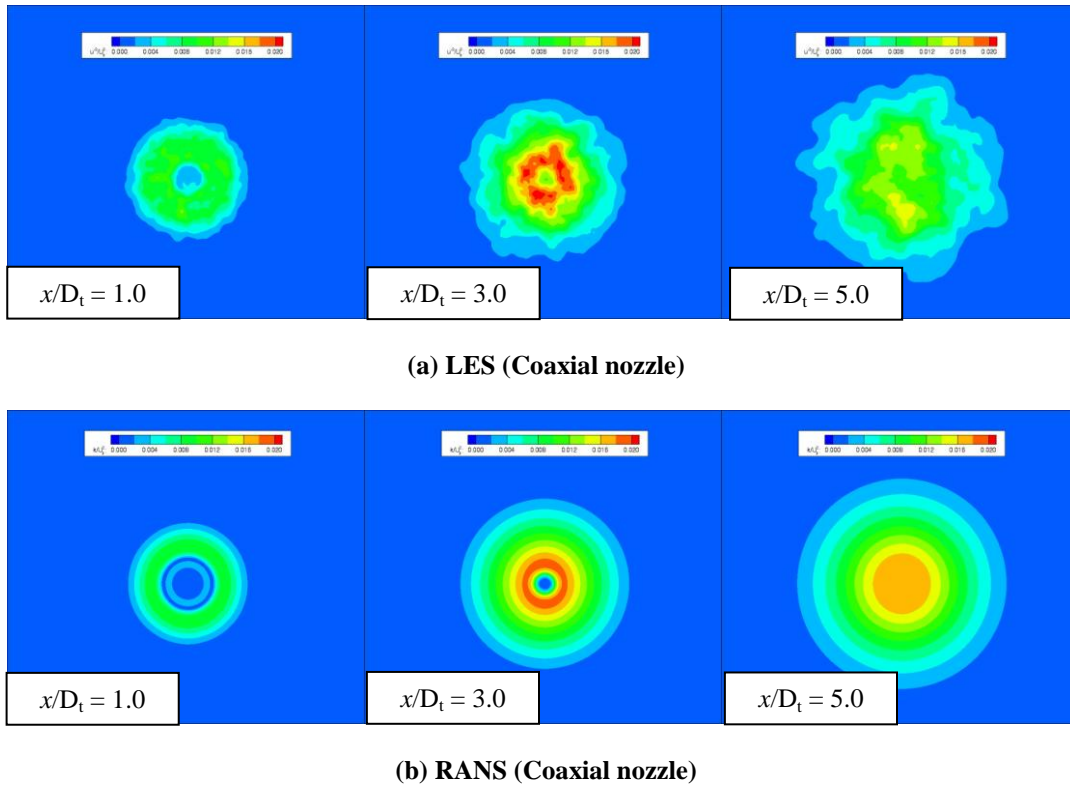
Fig. 13 Axial development of mean axial velocity along centerline.

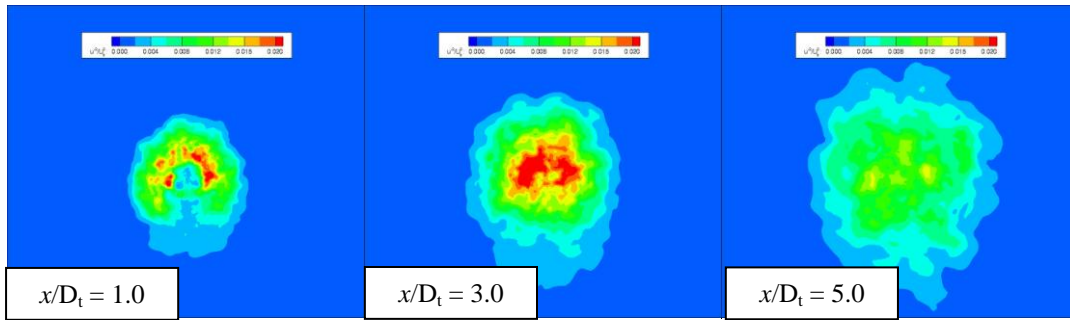
Figure 14 shows turbulent kinetic energy fields on the symmetry plane for the two nozzles at hot condition using the two computational approaches. Figure 15 shows the turbulent kinetic energy contours on three transverse planes. The two approaches show very similar turbulent kinetic energy fields and trends. Both of the methods show almost same peak turbulent kinetic energy locations and levels and

capture the substantial suppression of turbulent kinetic energy on the underside of the jet which results in the directional noise reduction. Note that the LES results are not smooth due to the limited number of time steps available.

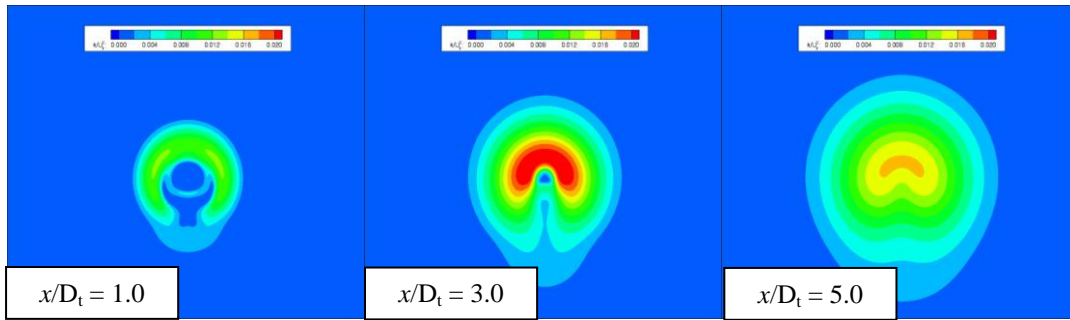


**Fig. 14** Turbulent kinetic energy contours on the symmetry plane for the three-stream jets. Left column shows the coaxial nozzle. Right column shows the asymmetric nozzle.





(c) LES (Asymmetric nozzle)

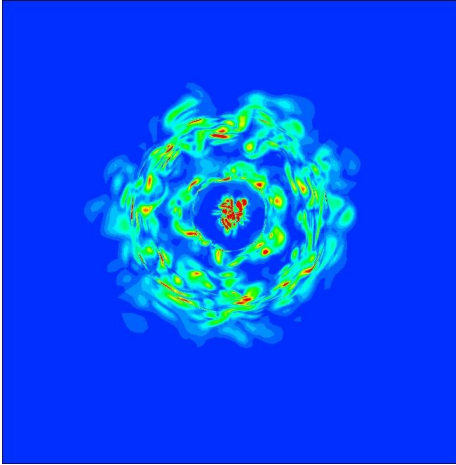


(d) RANS (Asymmetric nozzle)

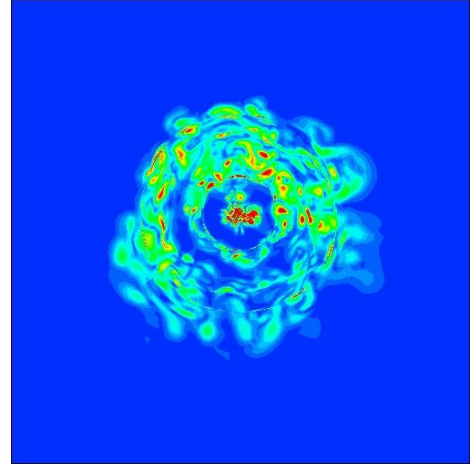
**Fig. 15 Time-averaged turbulent kinetic energy contours on the transverse planes.**

Figure 16 and 17 provides visual evidence of the favorable effect of offsetting the tertiary stream, showing the significant suppression of vorticity Magnitude and Mach waves on the underside of the asymmetric jet.

The aerodynamic performance of the nozzle was evaluated using a control volume that surrounded the entire nozzle<sup>19</sup>. Based on the predictions, the specific thrust loss of the asymmetric nozzle is about 0.039% which is considered small enough for practical application.

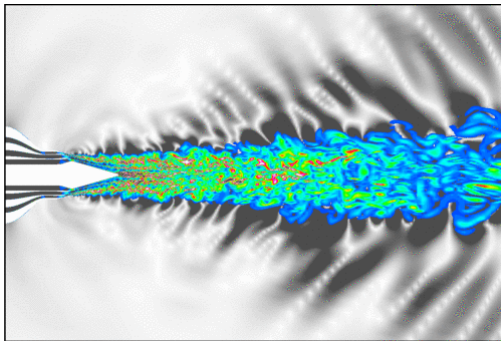


(a) Coaxial nozzle

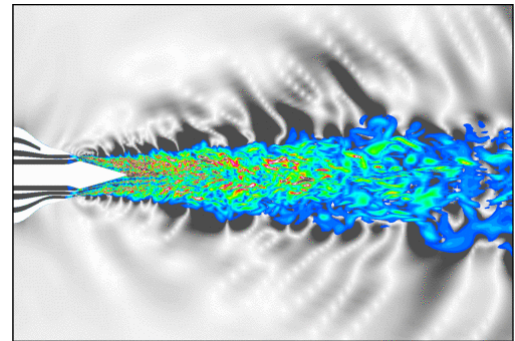


(b) Asymmetric nozzle

Fig. 16 LES results of instantaneous vorticity magnitude contours on transverse plane ( $x/D_t = 1.0$ )



(a) Coaxial nozzle



(b) Asymmetric nozzle

Fig. 17 LES results of instantaneous pressure contours  $|(p/p_a - 1)| < 0.0004$  (black and white scale) and vorticity magnitude contours (color scale) on symmetry plane.

### C. Far-Field Noise Prediction

The far-field noise was computed by surface integral using the Ffowcs Williams-Hawkings (FWH) formulation without external quadrupoles. The far field pressure is then expressed as the sum of monopole and dipole noise sources<sup>20</sup>. Figure 18 depicts the geometry of the FWH surface used for computing the radiated sound. The FWH surface extended to  $30D_t$  downstream. Here 2000 points in time were used with  $\Delta t = 50 \mu s$  for far field noise prediction. The predictions of the far-field sound pressure levels are compared with experimental measurements in Fig. 19 for axial nozzle. The comparisons of far-field sound pressure levels for asymmetric nozzle at downward direction and sideline direction (azimuth angle  $60^\circ$ ) are shown in Fig. 20 and Fig. 21. The far field noise experiment measurement setup was presented in Ref.8. The LES predicts a slightly lower pressure level than experimental measurements.

Overall, the LES/FWH scheme captures the trends of the pressure spectra at the two polar angles for the axial and asymmetric nozzles at downward and sideline directions. The predictions show the large far-field noise reduction for the low polar angle in the medium to high frequency range and minor noise increase for the high polar angle for the asymmetric nozzle compared with axial nozzle at downward direction. At sideline direction the predictions show a minor noise increase for the both polar angle in the high frequency range for the asymmetric nozzle compared with axial nozzle.

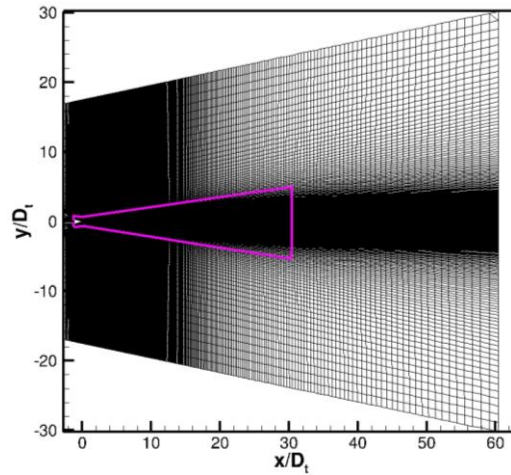
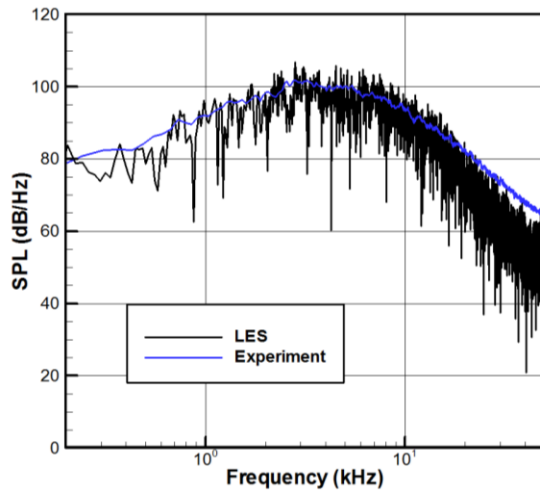
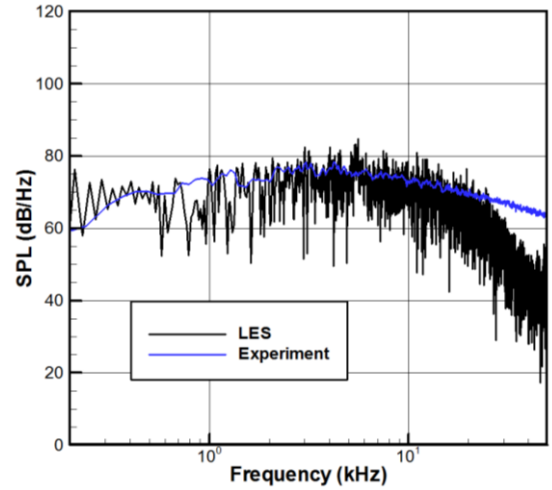


Fig. 18 FWH integral surface.

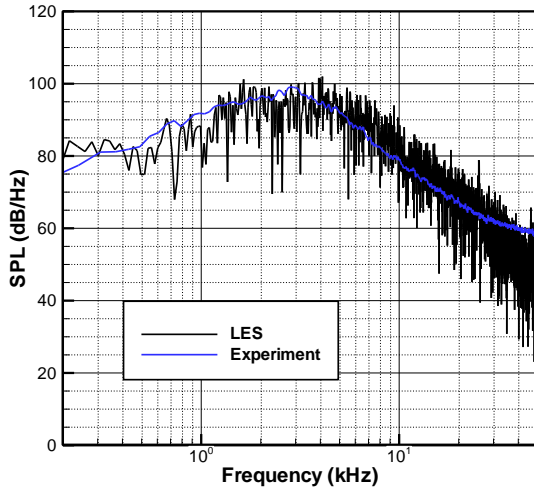


(a)  $\theta = 28.9^\circ$

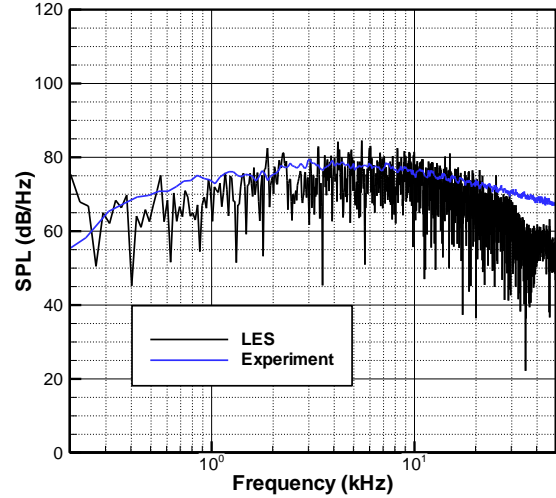


(b)  $\theta = 96.5^\circ$

Fig. 19 Far-field sound pressure level spectra for coaxial nozzle at different polar angles  $\theta$  with respect to the jet axis.

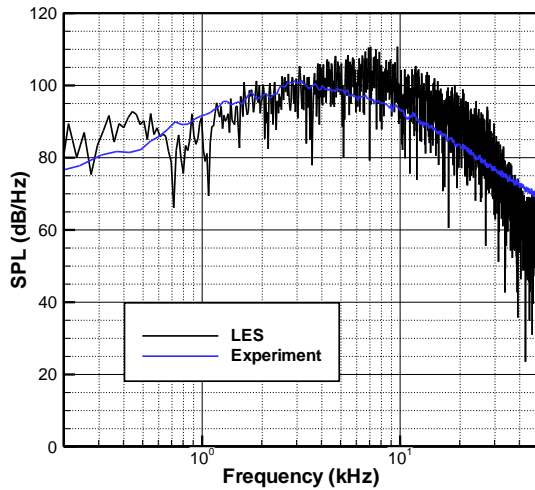


(a)  $\theta = 28.9^\circ$

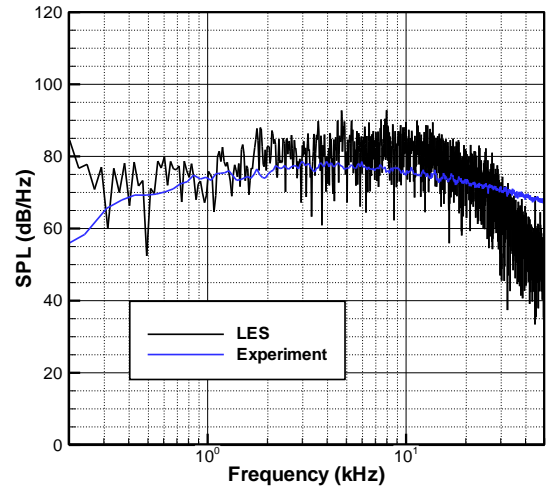


(b)  $\theta = 96.5^\circ$

**Fig. 20** Far-field sound pressure level spectra for asymmetric nozzle at different polar angles  $\theta$  with respect to the jet axis. (Downward direction)



(a)  $\theta = 28.9^\circ$



(b)  $\theta = 96.5^\circ$

**Fig. 21** Far-field sound pressure level spectra for asymmetric nozzle at different polar angles  $\theta$  with respect to the jet axis. (Sideline direction azimuth angle  $60^\circ$ )

#### IV. Conclusions

We presented a computation investigation of three-stream nozzle using LES and RANS approaches. The aim of the investigation was to help to fully understand the noise reduction mechanism of the

asymmetric nozzle scheme and enable to build a fast and accurate quantitative noise prediction mode. The computational validation was performed by comparing mean velocity fields for the jets at cold condition. Then the comparisons of the simulation results of time-average velocity and turbulent kinetic energy fields of the jets at cycle point hot between LES and RANS are performed. Both methods show qualitatively similar results. Asymmetric delivery of the tertiary stream shows strong reduction of turbulent kinetic energy, vorticity magnitude, and strength of the propagation waves. Far field noise prediction based on LES data shows reasonable comparison with experimental pressure spectra for the axial and asymmetric nozzles at downward and sideline directions. The asymmetric delivery of the tertiary stream shows large far-field noise reduction at peak noise emission polar angle at downward direction with minor noise increase at high polar angle at downward and sideline directions.

### **Acknowledgment**

We acknowledge the support by NASA Cooperative Agreement NNX 14AR98A, monitored Dr. James Bridges.

### **References**

1. Shur, M. L., Spalart, P. R., and Strlets, M. K., "LES-based evaluation of a microjet noise reduction concept in static and flight conditions," *Journal of Sound and Vibration*, Vol. 33, No. 13, 2011, pp. 4083-4097
2. Xia, H., Tucker, P. G., and Eastwood, S., "Large-eddy simulation of chevron jet flows with noise predictions," *International Journal of Heat and Fluid Flow*, Vol.30, 2009, 1067-1079
3. Mendez, S., Shoeybi, M., Sharma, A., Ham, F. E., Lele, S. K., and Moin, P., "Large-eddy simulation of perfectly-expanded supersonic jets: quality assessment and validation," AIAA Paper 2010-0271, Jan. 2010.
4. Uzun, A. and Hussaini, M. Y., "Simulation of noise generation in near-nozzle region of a chevron nozzle jet," *AIAA Journal*, Vol. 47, No.9, 2009, pp. 1793-1810.
5. Bogey, C. and Bailly C., "Large eddy simulation of round free jets using explicit filtering with/without dynamic Smagorinsky model," *International Journal of Heat and Fluid Flow*, Vol. 27, No.4, 2006, pp. 603-610.
6. Uzun, A., Lyrintzis, A. S., Blaisdell, G. A., "Coupling of Integral Acoustics Methods with LES for Jet Noise Prediction," *Journal of Aeroacoustics*, Vol. 3, No.4, 2004, pp. 297-346.
7. Verriere, J., Gand, F., and Deck, S., "Zonal Detached-Eddy Simulations of a Dual-Stream Jet," *AIAA Journal*, Vol. 54, No.10, 2016, pp. 3176-3190.
8. Papamoschou, D., Phong, V., Xiong, J., and Liu, F., "Quiet Nozzle Concepts for Three-Stream Jets," AIAA Paper 2016-0523, Jan. 2016.
9. Ffowcs Williams, J.E., and Hawkings, D.L., "Sound Generated by Turbulence and Surfaces in Unsteady Motion ", *Philosophical Transactions of the Royal Society*, 1969, A264 (1151), 321-342

10. Xiong, J., Johnson, A., Liu, F., and Papamoschou, D., "Body Force Model for the Aerodynamics of Inclined Perforated Surfaces," *AIAA Journal*, Vol. 50, No.11, Nov. 2012. pp. 2525-2535.
11. Jameson, A., Schmidt, W., and Turkel, E., "Numerical Solutions of the Euler Equations by Finite Volume Methods Using Runge-Kutta Time Stepping Schemes," AIAA 1981-1259, Jan. 1981.
12. Menter, F., "Two-Equation Eddy-Viscosity Turbulence Models for Engineering Applications," *AIAA Journal*, Vol. 32, No. 8, 1994, pp. 1598–1605.
13. Xiong, J., Nielsen, P., Liu, F., and Papamoschou, D., "Computation of High-Speed Coaxial Jets with Fan Flow Deflection," *AIAA Journal*, Vol. 48, No.10, 2010, pp. 2249-2262.
14. Shur, M. L., Spalart, P. R., and Strelets, M. K., "Noise Prediction for Increasingly Complex Jets. Part I: Methods and Tests," *International Journal of Aeroacoustics*, Vol. 4, No. 3, 2005, pp. 213–246.
15. Shur, M. L., Spalart, P. R., Strelets, M. K. and Garbaruk, A. V. "Further Steps in LES-Based Noise Prediction for Complex Jets," AIAA 2006-485, Jan. 2006.
16. Roe, P. L., "Approximate Riemann Solvers, Parameter Vectors and Difference Schemes," *Journal of Computational Physics*, Vol. 46, No. 2, 1980, pp. 357–378
17. Spalart, P. R. and Allmaras, S. R., "A One-Equation Turbulence Model for Aerodynamic Flows," AIAA 1992-0439, Jan. 1992.
18. Papamoschou, Xiong, J., and Liu, F., "Towards a Low-Cost Wavepacket Model of the Jet Noise Source," AIAA Paper 2015-1006, Jan. 2015.
19. Xiong, J., Liu, F., and Papamoschou, D., "Aerodynamic Performance of Fan Flow Deflectors for Jet Noise Reduction," *Journal of Propulsion and Power*, Vol. 28, No.4, 2012, pp. 728–738.
20. Papamoschou, D., "Modeling of Noise Reduction in Complex Multistream Jets," AIAA-2017-0001, Jan. 2017.